Frontiers of Information Technology & Electronic Engineering
www.jzus.zju.edu.cn; engineering.cae.cn; www.springerlink.com
ISSN 2095-9184 (print); ISSN 2095-9230 (online)
E-mail: jzus@zju.edu.cn

Single-layer chiral metasurface for circularly polarized light detection*

Xinjie SUN†§, Xin HE§, Zixin CAI, Xiang HAO†‡

College of Optical Science and Engineering, Zhejiang University, Hangzhou 310027, China

†E-mail: sunxj@zju.edu.cn; haox@zju.edu.cn

Received Feb. 3, 2024; Revision accepted May 1, 2024; Crosschecked

Abstract: Circular polarizers based on the metasurface suffer from the trade-off between the structural complexity and the polarization extinction ratio. Herein, we present a single-layer chiral metasurface with strong circular dichroism. The structure turns a circularly polarized incident beam into a linearly polarized one, achieving a high circular polarization extinction ratio. The operating wavelength of the proposed metasurface is tunable by changing the geometric parameters. Localized surface plasmon resonances between structures guarantee strong chiral optical effects of the metasurface. We further experimentally demonstrated the circular dichroism of the fabricated metasurface.

Key words: Optical metasurface; Polarization detection; Flat optical elements; Chiral metasurface
https://doi.org/10.1631/FITEE.2400081 **CLC number:**

1 Introduction

Polarization is critical for light. In particular, circularly polarized light (CPL) is widely used in holography (Wan et al.,2022; Wang et al., 2018), bio-imaging, optical communication (Farshchi et al.,2011), and many other advanced optical technologies (Lin et al.,2004; Garcia et al., 2015). The detection of CPL has a high potential for the development of these optical technologies. Traditional optical CPL detection requires a quarter-wave plate, a linear polarizer, and other mechanically rotating components. It causes substantial losses of sensitivity and resolution in light detection. Yet, the progress in optical metasurfaces provides opportunities for ultrathin CPL detection and manipulation.

The optical metasurfaces are the artificial electromagnetic media structured on the subwavelength scale, exhibiting unprecedented properties. Over the past few years, optical metasurfaces have been employed for the design and fabrication of optical elements and systems with abilities that surpass the performance of conventional optical elements (Pendry et al.,2006; Soukoulis and Wegener, 2010; Yu et al.,2011; Frese et al., 2019).

Specifically, for polarization applications, the 3D chiral optical metasurface was first proposed to differentiate the handedness of CPL (Hentschel et al.,2017), performing a wider regulation bandwidth and a higher circular polarization extinction ratio (ER). For example, the gold helix achieves an ER of 20 over a wide wavelength range (Gansel et al.,2010). The spiral-type ramp-shaped metamaterial (Rajaei et al.,2019) and the L-shaped metallic strip can also achieve optical chirality (Dietrich et al.,2012).

§ These authors contribute equally.
‡ Corresponding author
* Project supported by National Key R&D Program of China (No. 2022YFB3206000), the Fundamental Research Funds for the Central Universities (No. 2022QZJH29), National Natural Science Foundation of China (Nos. 92050115 and 42201336), and Zhejiang Provincial Natural Science Foundation of China (No. LZ21F050003)
ORCID: Xinjie SUN, https://orcid.org/0000-0003-0463-9074; Xin HE, https://orcid.org/0000-0002-5843-0332; Zixin CAI, https://orcid.org/0009-0001-2076-5997; Xiang HAO, https://orcid.org/0000-0002-3931-6884

Three-dimensional structures achieve high ERs and broad bandwidths. However, the fabrication of these complicated nanostructures has a high requirement for the equipment and the fabrication procedure, which is a fatal limitation to mass production.

With the development of nanotechnology, planar lithography techniques, such as photolithography and electron-beam lithography, have become mature, and the multi-layer metasurface dominates the research on artificial nanostructures for CPL detection. Multi-layer metasurfaces realize circular dichroism by rotating components of each layer or combining diverse metasurfaces to form a 3D chiral structure (Yun et al.,2017; Wang et al., 2016; Zhao et al.,2012; Zhao et al., 2022; Bai et al., 2019; Cen et al.,2022; Gorkunov et al., 2020). The ER of the multi-layer metasurface can reach 35 in experiments (Basiri et al.,2019). However, the multi-layer also suffers from fabrication challenges. For example, aligning vertically adjacent layers always requires a complex fabrication procedure involving multiple lithography and film deposition steps.

Single-layer structures can also be chiral and present circular dichroism, providing an alternative that has a simplified fabrication procedure. However, they always suffer from relatively low ERs in simulation (under 20) (Ma et al.,2018; Li et al., 2015; Zhang et al.,2017).

To resolve this dilemma, we developed a single-layer chiral metasurface that performs better cir-

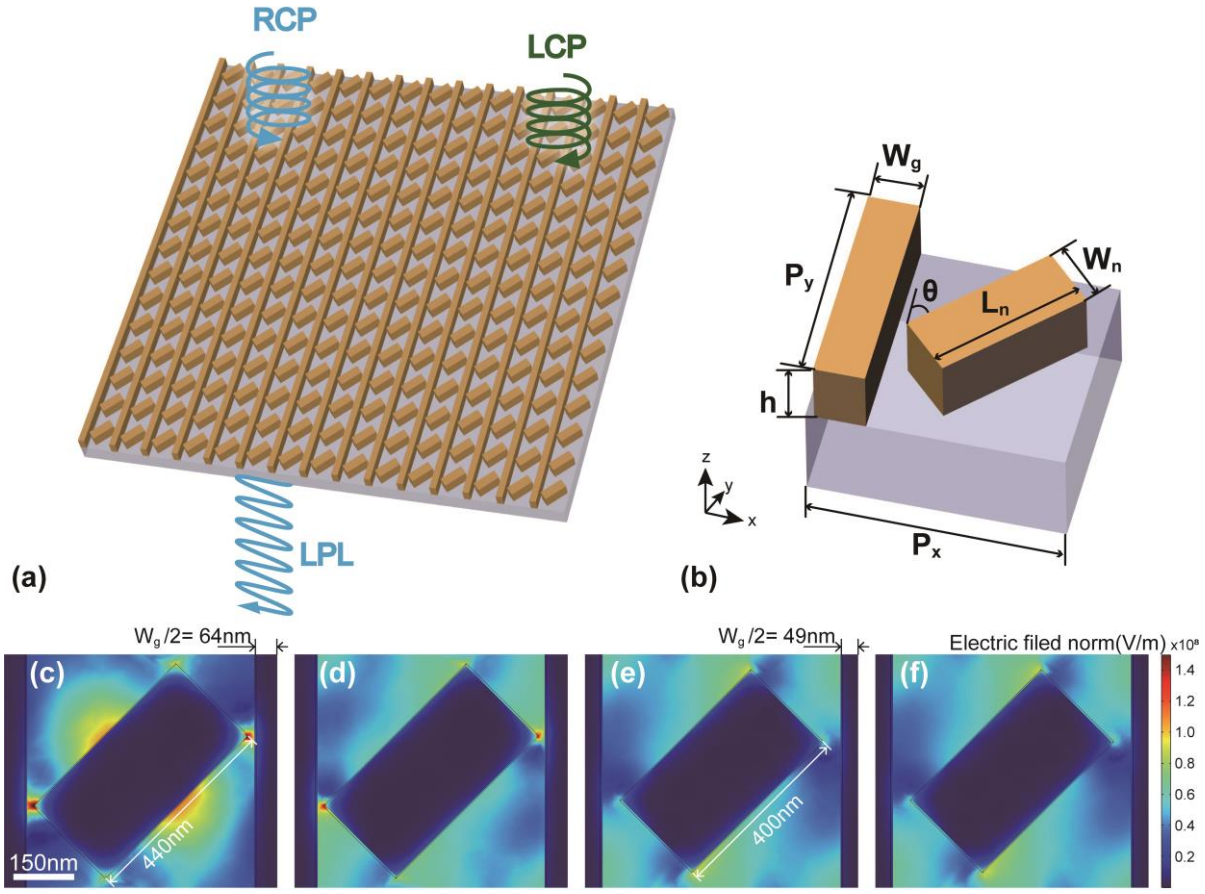

Fig.1. Schematic illustration of our single-layer metasurface circular polarizer. A right-handed circular polarizer selectively transmits right circularly polarized (RCP) light and converts it into linearly polarized light (LPL). (a) Overview of our metasurface. (b) Schematic of a single meta-molecule. The periods of meta-molecules are Px and Py along the x-axis and y-axis, respectively. Nano-gratings have a width (Wg). Rectangular nanorods rotate by θ = 45°with respect to nano-gratings and have a width (Wn) and a length (Ln). Their thickness is h. (c, d) Simulated electric field for left circularly polarized (LCP) illumination (c) and RCP (d) illumination of the metasurface whose operating wavelength is 840 nm. (e, f) Simulated electric field for 840 nm LCP (e) and RCP (f) illumination of the metasurface with geometric parameters slightly adjusted compared to those of the metasurface in (c, d).

cular dichroism and demonstrated it both in theory and through experiments. The operating wavelength of the proposed metasurface is tunable by changing the geometric parameters. The mechanism of high ER was explored through the simulated electric field and the component analysis of the transmitted light. In addition, we fabricated the structure and verified the circular dichroism of the proposed single-layer chiral metasurface in experiments. We further analyzed the reason for the difference between the simulation and the experiment.

2 Design and simulation

We applied the Jones matrix to characterize the polarization state conversion through the given interface. The transmission matrix of the conversion between a circularly polarized base and a linearly polarized base is described as:

$$T_{cir}=\begin{pmatrix} t_{rr} & t_{rl} \\ t_{lr} & t_{ll} \end{pmatrix} = \frac{1}{2}\begin{pmatrix} (t_{xx}+t_{yy})+i(t_{yx}-t_{xy}) & (t_{xx}-t_{yy})-i(t_{xy}+t_{yx}) \\ (t_{xx}-t_{yy})+i(t_{xy}+t_{yx}) & (t_{xx}+t_{yy})-i(t_{xy}-t_{yx}) \end{pmatrix}, \tag{1}$$

where r and l in the subscripts represent the right circularly polarized (RCP) and the left circularly polarized (LCP) light, respectively. The first and the second subscript denote the polarization of transmitted light and the incident one in sequence. Circular dichroism arises when $T_L \neq T_R$. The transmission of LCP and RCP incidence T_L and T_R are given by:

$$T_L = T_{LL} + T_{RL} = |t_{ll}|^2 + |t_{rl}|^2 \tag{2}$$

$$T_R = T_{RR} + T_{LR} = |t_{rr}|^2 + |t_{lr}|^2 . \tag{3}$$

For any single-layer metasurface with in-plane mirror symmetry, the Jones matrix is diagonalized so that the cross-polarization transmission coefficients $t_{xy} = t_{yx} = 0$ (Menzel et al.,2010). This indicates that no polarization state conversion occurs on this structure, and the circular dichroism is zero since $T_L = T_R$. To break the structural symmetry and create the dichroism, we employed the chiral metasurface, which is not consistent with its mirror structure by any azimuthal angle. We define the circular polarization extinction ratio (ER) as:

$$ER = T_{RCP}/T_{LCP} \tag{4}$$

to quantify the circular dichroism of the structure.

Fig. 1 shows our single-layer metasurface circular polarizer, which is composed of gold nano-gratings and a nanorod array. The unit cell of the metasurface (Fig. 1b) is designed as a chiral structure to generate strong circular dichroism via asymmetric metallic plasmonic distribution. The period of the array is sub-wavelength to avoid high-order diffraction. SiO_2 is used as the substrate. Between the substrate and the gold layer lies a 5-nm-thick Cr adhesive layer. The gratings are along the *y*-axis, while the rectangular nanorods rotate 45° from the gratings and are repeated along the *x*- and the *y*-axes. Remarkably, the handedness of the metasurface polarizer is switchable, depending on the selective absorption of the polarization component. When LCP absorption dominates ($\theta = 45^\circ$), our metasurface acts as a right-handed polarizer, whereas it converts to a left-handed one when $\theta = -45^\circ$. It should be noted that there is nearly no difference in simulation results between the right-handed and left-handed polarizers. Therefore, this article only presents and analyzes the results of the right-handed polarizer.

We chose this single-layer chiral structure since its localized surface plasmon resonances (LSPR) distribution is polarization-dependent. This phenomenon in turn triggers strong circular dichroism. To understand the underlying mechanism, we simulated the near-field electric distribution around the metasurface under the illumination light with different circular polarization states (Figs. 1c-1d). For the LCP illumination shown in Fig. 1c, the strong electric field appears in the middle of the long side for the rectangular nanorods, which results in a high absorption. In contrast, for the RCP illumination (Fig .1d), the electric field is weaker but has a more uniform distribution. In this way, our metasurface allows selective polarization transmission and conversion.

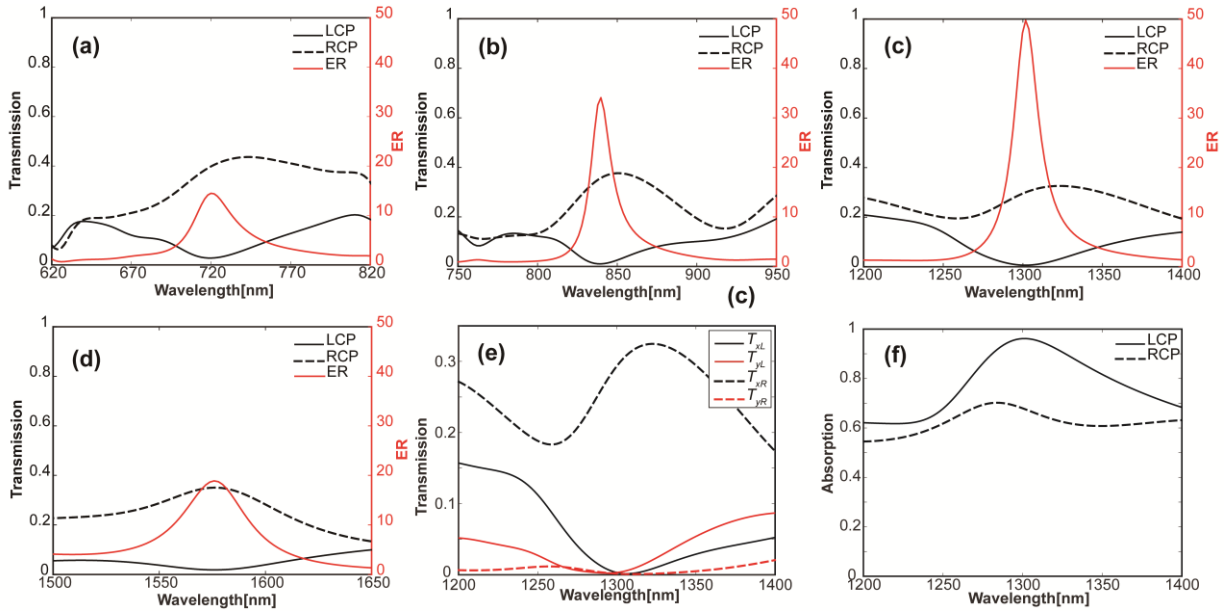

Fig. 2. Simulation results as a function of operating wavelength. (a - d) Transmission of LCP and RCP light (black solid/dashed lines and left y-axis) and ERs (red solid lines and right y-axis) of the metasurfaces working at (a) 720 nm, (b) 840 nm, (c) 1300 nm, and (d) 1580 nm, respectively. (e) Transmittance coefficients of linear polarization when the incident light is circularly polarized. (f) Absorption spectra for LCP and RCP incidences.

Notably, the performance of our metasurface is closely related to the geometric parameters. When these parameters deviate from the optimal values (40 nm decrease in L_n and 30 nm decrease in W_g compared with Figs. 1c-1d), the intensity of LSPR, which exists around the nanorod, is dramatically weakened (Figs. 1e-1f) and the ER decreases from 34 to 14. These two electric fields shown in Figs. 1e-1f under illuminations with different handedness do not differ significantly, thereby impairing the circular dichroism of our metasurface. Based on the proposed structure, we present the optimal values of geometric parameters of four operating wavelengths in Table 1. We intentionally kept all minimum distances between the nano-grating and the nanorod above 20 nm to guarantee that the pattern is producible using electron beam lithography (EBL). For quantitative analysis, we further calculated their corresponding ERs using full-wave simulations (Fig. 2). In Figs. 2a-2d, the solid black and dashed lines represent the transmission of LCP and RCP incidence, respectively, and the solid red lines represent ERs. In general, the ER values are consistent with the theoretical prediction. The transmission of specific-handed CPL can be close to 0, whereas its orthogonal component maintains a higher transmission, realizing an ER peak around the desired operating wavelength. For example, as shown in Fig. 2c, when the wavelength is 1300 nm, the transmission of LCP and RCP light is 0.006 and 0.30, respectively, resulting in a peak ER value of 50. A similar trend is also visible in Figs. 2a-2d. Remarkably, besides the four operating wavelengths mentioned above, this model can de facto cover the visible to near-infrared range (700–1600 nm).

We made a deeper investigation into the optical response of our metasurface operating at 1300 nm. Fig. 2e shows the transmission of linearly polarized components when the incident light is circularly polarized. The *x*-polarized component has a higher transmission compared to the *y*-polarized one, which

Table 1. Key parameters of metasurface for simulation.

Operating wavelength(nm)	Simulated ER	P_x(nm)	P_y(nm)	W_g(nm)	W_n(nm)	L_n(nm)	h(nm)
720	15	640	600	128	180	440	200
840	34	840	720	143	310	610	200
1300	50	1350	980	135	500	720	350
1580	18	1550	1200	155	600	1050	400

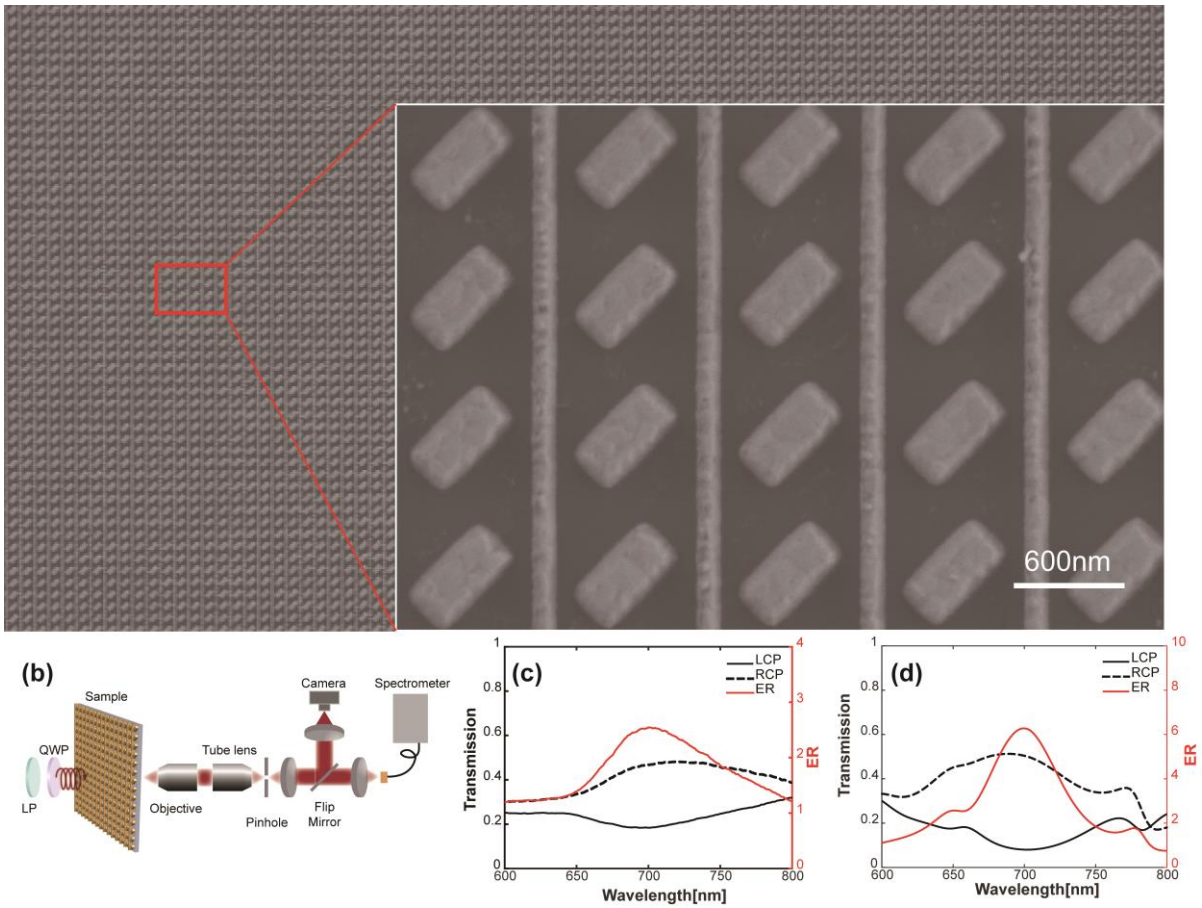

Fig. 3. Fabrication and characterization of our single-layer metasurface circular polarizer. (a) Scanning electron microscope images of the right-handed fabricated metasurface. (b) Schematic of the experimental setup. (c) Measured optical properties of our metasurface circular polarizer, and (d) the simulation results of the metasurface adjusting its geometric parameters according to the fabricated metasurface. In these two graphs, the transmission of LCP (black solid line) and RCP (black dashed line) light correspond to the principal axis on the left, while the scale of ER (red solid line) is shown as the secondary axis on the right. Abbreviations: LP, linear polarizer; QWP, quarter-wave plate.

is determined by the orientation of the nano-gratings in the metasurface (Basiri et al.,2019). In particular, at a wavelength of 1300 nm, the transmission of *x*-polarized light is 0.3, whereas the *y*-polarized one is almost zero. The planar chirality of the metasurface causes cross-polarization conversion to differentiate the transmission of LCP and RCP incidence. For the incident light, 96% of the LCP component is absorbed (Fig. 2f). Therefore, our metasurface polarizer converts the RCP incidence to linearly polarized light (LPL) at high efficiency but absorbs the LCP component.

3 Fabrication and results

To demonstrate our metasurface circular polarizer on a challenging target for fabrication, we opted for 720 nm as the operating wavelength with the smallest feature sizes (Table 1). We fabricated a right-handed array based on a silica substrate. A 5-nm-thick Cr adhesive layer followed by a 200-nm-thick gold layer was deposited on the silica substrate by the high vacuum evaporation system (ei-5z). The pattern was fabricated by EBL (RAITH VOYAGER). Fig. 3a shows the scanning electron microscope (SEM) image of the fabricated metasurface.

To characterize the transmission of the fabricated metasurface, we used a custom spectrometer integrated into a microscope (Fig. 3b). The unpolarized light from a halogen tungsten lamp was converted by a combination of a linear polarizer (LP) and a quarter-wave plate (QWP) into the CPL to illuminate the sample. The transmitted light was gathered by the microscope and then detected by a spectrom-

eter. A flip mirror was set between the lenses to reflect the light into the camera as needed.

The measured results are shown in Fig. 3c. In brief, the transmission of LCP is lower than RCP, which is consistent with the simulation. The measured transmitted spectra also perform the discrimination of different handedness illumination as expected. The measured peak ER reaches 2.5. This value is lower than that in simulation, mainly due to the deviation during the multi-step fabrication. Due to the limitation of fabrication accuracy, to keep a clear gap between the nano-grating and the nanorod, SEM measured the gap as being enlarged to 80 nm during the actual processing, instead of 37 nm as the design. This is mainly because the manufacturing accuracy of the EBL is not high enough. To demonstrate the impact of manufacturing errors, we adjusted the geometric parameters of the metasurface operating at 720 nm, as shown in Table 1, to match the measured parameters of the fabricated metasurface in Fig. 3a. Fig 3d illustrates the simulation results, confirming the influence of manufacturing errors on the metasurface's performance, indicated by a decrease in peak ER from 14.5 in Fig. 2a to 6.2 in Fig. 3d. Additionally, inaccurate fabrication led to a shift in the peak wavelength. However, it is feasible to fabricate 37 nm gaps and achieve a metasurface that better conforms to the designed parameters using higher precision equipment (Devlin et al.,2016). We were also aware that the roughness of the nano-gratings was up to 5 nm, which also decreased the device's performance. However, the peak position is still maintained, which validates our overall design.

4 Conclusion

We have designed and fabricated a single-layer chiral metasurface structure for CPL distinction. The metasurface converts a specific handed CPL into LPL and absorbs the orthogonal component. The single-layer chiral structure holds the promise of high ER. It can work from 700 nm to 1600 nm by tuning the geometric parameters. Four examples working at 720 nm, 840 nm, 1300 nm, and 1580 nm are shown in this paper. The ability to convert one specific-handed CPL into LPL stems from the nano-gratings and the chiral plasmonic structure. Our experimental results demonstrate the circular dichroism of the proposed chiral metasurface. However, there is still room for improvement during the fabrication process. Our work holds the promise of high ER, tunable operation, simple fabrication, and integration. It can be applied to fiber optics, chip-integrated systems for quantum computing, polarimetric detectors, and emission and sensing applications for CPL.

Contributors

Xinjie SUN, Xin HE, and Xiang HAO designed the research. Xinjie SUN processed the data, performed the theoretical analysis and the measurement of the sample, and drafted the paper. Xinjie SUN and Xin HE fabricated the samples. Zixin Cai helped organize the paper. Xinjie SUN, Xin HE, and Xiang HAO revised and finalized the paper.

Acknowledgements

This work was partially carried out at the Micro-Nano Fabrication Center of Zhejiang University. We also thank the Westlake Center for Micro/Nano Fabrication for facility support and technical assistance.

Conflict of interest

All the authors declare that they have no conflicts of interest.

Data availability

Data underlying the results presented in this paper are not publicly available at this time but may be obtained from the authors upon reasonable request.

References

Bai J, Wang C, Chen XH, et al., 2019. Chip-integrated plasmonic flat optics for mid-infrared full-Stokes polarization detection. *Photonics Res*, 7(9):1051-1060. https://doi.org/10.1364/PRJ.7.001051

Basiri A, Chen XH, Bai J, et al., 2019. Nature-inspired chiral metasurfaces for circular polarization detection and full-Stokes polarimetric measurements. *Light: Sci Appl*, 8:78. https://doi.org/10.1038/s41377-019-0184-4

Cen MJ, Wang JW, Liu JX, et al., 2022. Ultrathin suspended chiral metasurfaces for enantiodiscrimination. *Adv Mater*, 34(37):2203956. https://doi.org/10.1002/adma.202203956

Devlin RC, Khorasaninejad M, Chen WT, et al., 2016. Broadband high-efficiency dielectric metasurfaces for the visible spectrum. *Proc Natl Acad Sci USA*, 113(38):10473-10478. https://doi.org/10.1073/pnas.1611740113

Dietrich K, Lehr D, Helgert C, et al., 2012. Circular dichroism from chiral nanomaterial fabricated by on-edge lithography. *Adv Mater*, 24(44):OP321-OP325. https://doi.org/10.1002/adma.201203424

Farshchi R, Ramsteiner M, Herfort J, et al., 2011. Optical communication of spin information between light emitting diodes. *Appl Phys Lett*, 98(16):162508. https://doi.org/10.1063/1.3582917

Frese D, Wei QS, Wang YT, et al., 2019. Nonreciprocal asymmetric polarization encryption by layered plasmonic metasurfaces. *Nano Lett*, 19(6):3976-3980. https://doi.org/10.1021/acs.nanolett.9b01298

Gansel JK, Wegener M, Burger S, et al., 2010. Gold helix photonic metamaterials: a numerical parameter study. *Opt Express*, 18(2):1059-1069. https://doi.org/10.1364/OE.18.001059

Garcia NM, de Erausquin I, Edmiston C, et al., 2015. Surface normal reconstruction using circularly polarized light. *Opt Express*, 23(11):14391-14406. https://doi.org/10.1364/OE.23.014391

Gorkunov MV, Antonov AA, Kivshar YS, 2020. Metasurfaces with maximum chirality empowered by bound states in the continuum. *Phys Rev Lett*, 125(9):093903. https://doi.org/10.1103/PhysRevLett.125.093903

Hentschel M, Schäferling M, Duan XY, et al., 2017. Chiral plasmonics. *Sci Adv*, 3(5):e1602735. https://doi.org/10.1126/sciadv.1602735

Li W, Coppens ZJ, Besteiro LV, et al., 2015. Circularly polarized light detection with hot electrons in chiral plasmonic metamaterials. *Nat Commun*, 6:8379. https://doi.org/10.1038/ncomms9379

Lin SS, Yemelyanov KM, Pugh EN, et al., 2004. Polarization enhanced visual surveillance techniques. IEEE International Conference on Networking, Sensing and Control, p.216-221. https://doi.org/10.1109/ICNSC.2004.1297437

Ma ZJ, Li Y, Li Y, et al., 2018. All-dielectric planar chiral metasurface with gradient geometric phase. *Opt Express*, 26(5):6067-6078. https://doi.org/10.1364/OE.26.006067

Menzel C, Rockstuhl C, Lederer F, 2010. Advanced Jones calculus for the classification of periodic metamaterials. *Phys Rev A*, 82(5):053811. https://doi.org/10.1103/PhysRevA.82.053811

Pendry JB, Schurig D, Smith DR, 2006. Controlling electromagnetic fields. *Science*, 312(5781):1780-1782. https://doi.org/10.1126/science.1125907

Rajaei M, Zeng JW, Albooyeh M, et al., 2019. Giant circular dichroism at visible frequencies enabled by plasmonic ramp-shaped nanostructures. *ACS Photonics*, 6(4):924-931. https://doi.org/10.1021/acsphotonics.8b01584

Soukoulis CM, Wegener M, 2010. Optical metamaterials—more bulky and Less Lossy. *Science*, 330(6011):1633-1634. https://doi.org/10.1126/science.1198858

Wan WP, Yang WH, Ye S, et al., 2022. Tunable full-color vectorial meta-holography. *Adv Opt Mater*, 10(22):2201478. https://doi.org/10.1002/adom.202201478

Wang Q, Plum E, Yang QL, et al., 2018. Reflective chiral meta-holography: multiplexing holograms for circularly polarized waves. *Light: Sci Appl*, 7:25. https://doi.org/10.1038/s41377-018-0019-8

Wang ZJ, Jia H, Yao K, et al., 2016. Circular dichroism metamirrors with near-perfect extinction. *ACS Photonics*, 3(11):2096-2101. https://doi.org/10.1021/acsphotonics.6b00533

Yu NF, Genevet P, Kats MA, et al., 2011. Light propagation with phase discontinuities: generalized laws of reflection and refraction. *Science*, 334(6054):333-337. https://doi.org/10.1126/science.1210713

Yun JG, Kim SJ, Yun H, et al., 2017. Broadband ultrathin circular polarizer at visible and near-infrared wavelengths using a non-resonant characteristic in helically stacked nano-gratings. *Opt Express*, 25(13):14260-14269. https://doi.org/10.1364/OE.25.014260

Zhang F, Pu MB, Li X, et al., 2017. All-dielectric metasurfaces for simultaneous giant circular asymmetric transmission and wavefront shaping based on asymmetric photonic spin–orbit interactions. *Adv Funct Mater*, 27(47):1704295. https://doi.org/10.1002/adfm.201704295

Zhao X, Li ZC, Cheng JQ, et al., 2022. Realization of maximum optical intrinsic chirality with bilayer polyatomic metasurfaces. *Opt Lett*, 47(18):4814-4817. https://doi.org/10.1364/OL.469518

Zhao Y, Belkin MA, Alù A, 2012. Twisted optical metamaterials for planarized ultrathin broadband circular polarizers. *Nat Commun*, 3:870. https://doi.org/10.1038/ncomms1877